

AIE Supramolecular Polymeric Material Based on *t*Q[14]: Highly Sensitive Detection and Efficient Removal of Potential Cyanide from Water

Wei Zhang,^a Yang Luo,^a Pan-hua Zhu,^a Xin-long Ni,^a Carl Redshaw,^b Zhu Tao,^a and Xin Xiao,^{a*}

^a Key Laboratory of Macrocyclic and Supramolecular Chemistry of Guizhou Province, Institute of Applied Chemistry, Guizhou University, Guiyang 550025, China.

^b Department of Chemistry, University of Hull, Hull HU6 7RX, U.K.

Corresponding authors E-mail: gyhxxiaoxin@163.com (Xin Xiao).

KEYWORDS: Cucurbit[*n*]urils; AIE Supramolecular Polymers; Efficient removal; Sensitive Detection; Potential Cyanide

ABSTRACT: Potassium ferricyanide in an aqueous solution is easily decomposed into highly toxic substances (potassium cyanide and hydrogen cyanide) by light or alkaline action, which poses a major hazard to humans and environmental health. Here, a reticulated AIE supramolecular polymer material (TPAP-Mb@*t*Q[14]) was prepared by the supramolecular self-assembly of cucurbit[14]uril (*t*Q[14]) and a triphenylamine derivative (TPAP-Mb). TPAP-Mb@*t*Q[14] not only recognizes Fe(CN)₆³⁻ with ultrasensitive specificity with a LOD of 1.64×10⁻⁷ M, but can also effectively remove and adsorb Fe(CN)₆³⁻ from aqueous solution with a removal rate as high as

97.38%. Meanwhile, a significant component of the *t*Q[14] material can be recycled. Thus, the *t*Q[14]-based supramolecular assembly has the potential to be used for applications addressing toxic anionic contaminants present in aqueous environments.

SYNOPSIS: A green, recyclable AIE supramolecular polymeric material based on *t*Q[14] has potential applications in solving environmental water pollution problems.

INTRODUCTION

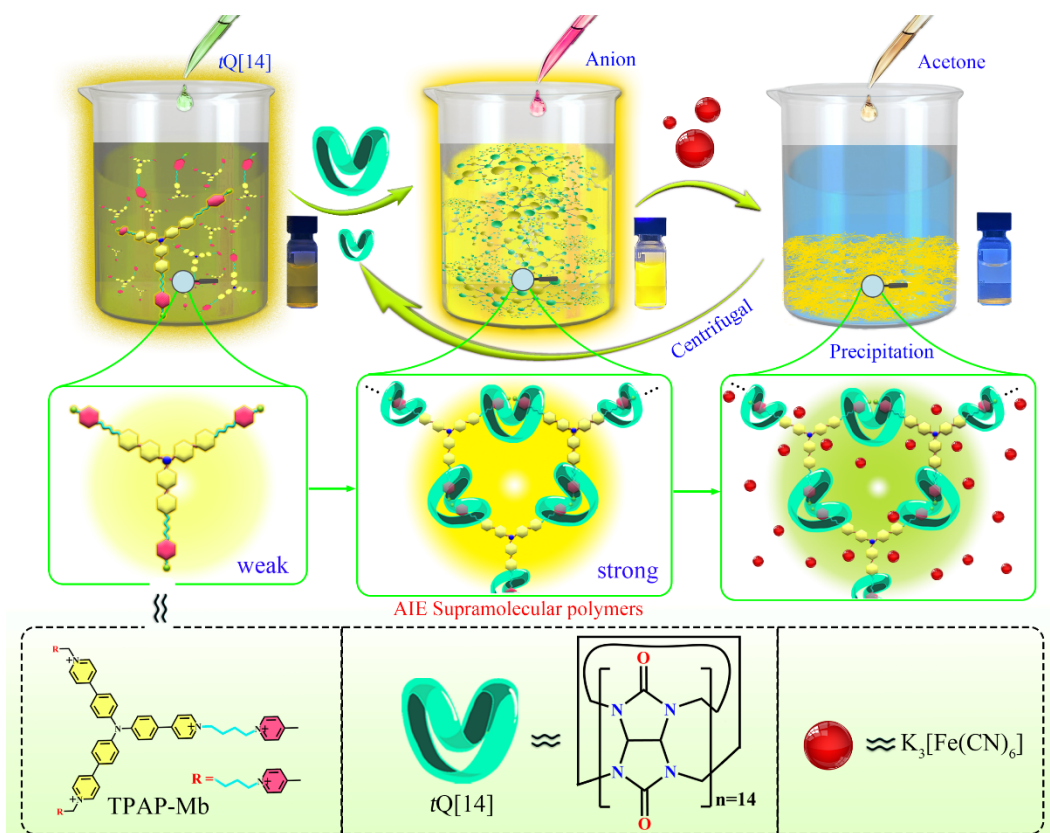
Anionic species play a crucial role in chemical, biological and environmental events, and more and more research groups are focusing on the identification of anions, which is rapidly developing into a new area of interest in supramolecular chemistry.¹⁻³ Potassium ferricyanide ($K_3[Fe(CN)_6]$) was discovered in 1822, the central atom of this substance is an iron ion (Fe^{3+}), and the ligands are cyanide ions (CN⁻); it is very stable as a solid at room temperature. Potassium cyanide can be produced by burning. In addition, $K_3[Fe(CN)_6]$ can also decompose when exposed to light and alkali in an aqueous solution, producing highly toxic cyanides (potassium cyanide and hydrocyanic acid)⁴⁻⁶ that pose a serious risk to the lives of aquatic organisms. Indeed, as a highly toxic substance, potassium cyanide can still pose a serious hazard to most organisms, including humans, even at very low concentrations. As a highly toxic substance, cyanide is highly harmful to most organisms, including humans, even at low concentrations. It can be absorbed by the skin, lungs and stomach, thereby binding to the active site of oxidative enzymes in cytochromes and inhibiting oxygen utilization, leaving tissues in a state of severe hypoxia, sufficient to cause the immediate death of the organism.⁷⁻¹¹ Therefore, the use of these highly toxic cyanides has been restricted on a large scale. However, the use of potassium ferricyanide cannot be avoided, as it is an important chemical in various industrial processes, including pharmaceuticals, metallurgy and pigments. Accidental

release of cyanide into water can lead directly to serious environmental problems and life-threatening health issues.¹²⁻¹⁴ The World Health Organization (WHO) requires that the maximum concentration of cyanide in drinking water does not exceed 1.9 μM ,¹⁵ which makes potassium ferricyanide in water a potential threat. Given this, the detection of potassium ferricyanide is a particularly important project. The advent of fluorescent chemical sensors has brought increased attention to the study of detecting $\text{Fe}(\text{CN})_6^{3-}$ in water, but most studies have not yet been able to achieve both the highly sensitive detection as well as the removal of $\text{Fe}(\text{CN})_6^{3-}$.¹⁶⁻¹⁸ Therefore, the development of novel materials for ultrasensitive detection and effective removal of cyanide in water is an important research topic in materials chemistry and environmental science.

In particular, it is recognized that the effective removal of cyanide in contaminated wastewater has not received sufficient attention so far and the development of sensors capable of high selectivity and removal in aqueous solutions remains a challenge.¹⁹⁻²¹ Conventional fluorescent sensors with bulky π -conjugated aromatic systems of emission groups often exhibit insolubility in water and produce ACQ phenomena in the aggregated state of aqueous solutions, making their optical properties poor and greatly limiting applications in aqueous solutions.²²⁻²⁴ Aggregation-induced emission (AIE) is an interesting optophysical phenomenon in which fluorophores exhibit enhanced fluorescence emission in the aggregated state.²⁵ In recent years, various AIE luminophores have been reported (neutral AIE luminophores, ionic AIE species, *etc.*),^{26,27} and such new supramolecular polymer materials with AIE properties have been constructed using dynamically reversible noncovalent interactions, which not only have good optical properties but also have ultrasensitive stimulus-responsive properties. In particular, the construction of supramolecular polymers with AIE properties based on macrocyclic compounds has received much attention in numerous fields, including biology²⁸ fluorescent sensors and the field of stimuli-

responsive materials.²⁹⁻³¹ Twisted cucurbit[14]uril (*t*Q[14])²²⁻³⁵ is a rare macrocyclic compound of the Q[*n*]s family and possesses good water solubility.³⁶⁻⁴³ Due to its two cavities capable of binding two of the same or different guests simultaneously, supramolecular polymers with different topologies can be constructed by further assembly.

Here, TPAP-Mb (1,1',1''-(((nitrilotris(benzene-4,1-diyl))tris(pyridine-1-ium-4,1-diyl))tris(butane-4,1-diyl))tris(4-methylpyridine-1-ium), [Figures S1-S7 and Scheme 1](#)) was successfully designed and synthesized based on the classical AIE molecule triphenylamine. TPAP-Mb is a tailor-made guest molecule for *t*Q[14], and its alkyl chain and methylpyridine fraction can easily interact with *t*Q[14] through host-guest interactions, thereby inducing the restriction of the intramolecular rotation (RIR) effect of TPAP-Mb, and finally constructing the AIE fluorescent supramolecular polymer (TPAP-Mb@*t*Q[14]). TPAP-Mb@*t*Q[14] can detect Fe(CN)₆³⁻ in an aqueous solution with an ultra-sensitive detection of limit (LOD) of up to 1.64×10⁻⁷ M. More importantly, TPAP-Mb@*t*Q[14] also can effectively remove K₃Fe(CN)₆ from aqueous solutions and the *t*Q[14] can be recovered in a recyclable fashion. Thus, AIE fluorescent supramolecular polymers constructed by host-guest interactions not only provide a new idea for the development of novel smart supramolecular materials for tackling environmental pollution but also have potential applications in the detection of cyanide and the efficient removal of cyanide from wastewater.



Scheme 1 Schematic illustration of the AIE supramolecular polymer formation process and anion removal.

EXPERIMENTAL SECTION

Some conventional experimental methods including fluorescence spectroscopy, NMR spectroscopy, electron microscopy (TEM and SEM), *etc.*, are recorded in detail in the [Supporting Information](#). Here, the synthesis of TPAP-Mb ([Scheme S1](#)) is described in detail. Tris(4-(1H-imidazol-1-yl)phenyl)amine (477 mg, 0.1 mmol) and 1-(4-bromobutyl)-4-methylpyridin-1-ium (942 mg, 0.31 mmol) were completely dissolved in 20 mL of $CH_3CN:DMF=20:1$ solution and refluxed for 12 h to form a yellow precipitate. After cooling to room temperature, the reaction mixture was repeatedly washed with acetonitrile and filtered and dried under vacuum to give a yellow solid in 68% yield. See the relevant [Supporting Information](#) for related representations.

RESULTS AND DISCUSSION

^1H NMR experiments were first used to study the interaction pattern of TPAP-Mb and $t\text{Q}[14]$ and the preliminary construction of supramolecular polymers (TPAP-Mb@ $t\text{Q}[14]$). The proton signals of TPAP-Mb were determined based on the 2D ^1H - ^1H COSY spectrum (Figure S4). As shown in Figure 1, after the gradual addition of $t\text{Q}[14]$ to TPAP-Mb, the protons on the methyl pyridine (δ_a - δ_c , δ_h) and butyl chains (δ_e - δ_g) were shifted upfield due to the shielding effect of the hydrophobic cavity of $t\text{Q}[14]$. On the contrary, the proton signal on the triphenylamine (δ_i - δ_k) was shifted downward field due to the de-shielding effect of the $t\text{Q}[14]$ -port. The above results indicate that the butyl chains and pyridine groups of the three ‘arms’ of TPAP-Mb enter the cavity of the $t\text{Q}[14]$, while the central part of the triphenylamine remains outside the cavity and is further assembled into a supramolecular polymer (TPAP-Mb@ $t\text{Q}[14]$) through host-guest interactions. Finally, isothermal titration calorimetry (ITC, Figure S8) further demonstrated the binding ability of TPAP-Mb@ $t\text{Q}[14]$ with a binding constant (K_a) of $(3.96 \pm 0.046) \times 10^{-11} \text{ M}^{-2}$.

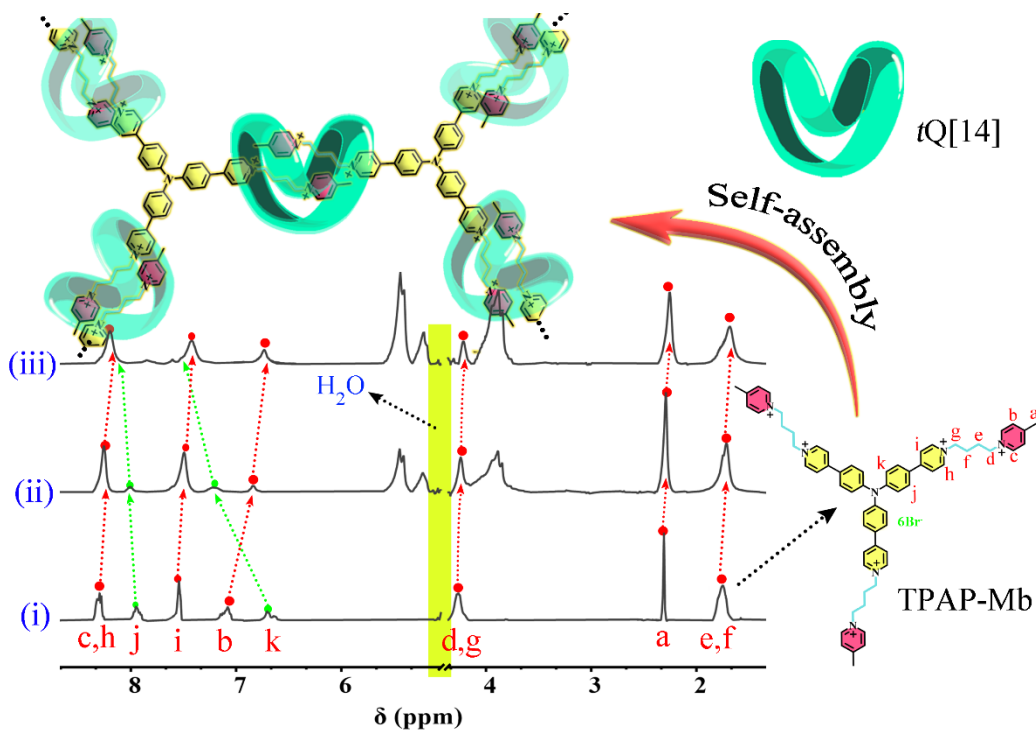


Figure 1 Illustration of the formation of TPAP-Mb@*t*Q[14] (top) ¹H NMR titration (D₂O, pD= 6.75, 298K) of TPAP-Mb at different concentrations of *t*Q[14] from 0 (i), 1.0 (ii) 2.0 (iii). The specific chemical shift data are shown in **Table S1**.

Given that TPAP-Mb is a classical triphenylamine derivative of the AIEgens type molecules, it is important to investigate its AIE behavior in different ratios of H₂O/CH₃CN solvents. As shown in **Figures 2a and b**, TPAP-Mb shows a very faint yellow fluorescence in the dispersed state ($f_{\text{acetonitrile}} < 91\%$), while TPAP-Mb undergoes aggregation and shows yellow fluorescence when the content of acetonitrile is 91-96% (inset **Figures 2b**). Subsequently, the spectral changes due to the effect of *t*Q[14] on TPAP-Mb were investigated by fluorescence titration experiments. With the gradual addition of *t*Q[14] to the TPAP-Mb solution, a dramatic increase in the fluorescence intensity at $\lambda_{\text{em}} = 572$ nm occurred (52.3 a.u. to 813.42 a.u.). At the same time, the color of the solution changed from a faint yellow light to bright yellow and a clear Tyndall phenomenon could be observed in the TPAP-Mb solution in the presence of *t*Q[14] under irradiation using a 365 nm UV lamp (inset **Figures 2c**). The sharp enhancement of fluorescence is attributed to the self-assembly of the alkyl chain and pyridine of TPAP-Mb with the two cavities of *t*Q[14] through host-guest interactions. The addition of *t*Q[14] restricts the intramolecular rotation and stacking of TPAP-Mb, making the molecular excited-state energy less susceptible to dissipation, which favors the occurrence of a radiative leap, leading to a pronounced AIE effect. In addition, the Job's plots of TPAP-Mb with *t*Q[14] and UV-Vis titration experiments confirmed the molar ratio of TPAP-Mb:*t*Q[14] = 2:3 (**Figure 2d and Figure S10**). The above results indicate that TPAP-Mb and *t*Q[14] initially construct supramolecular polymers with an AIE effect through host-guest interactions and exhibit good optical properties.

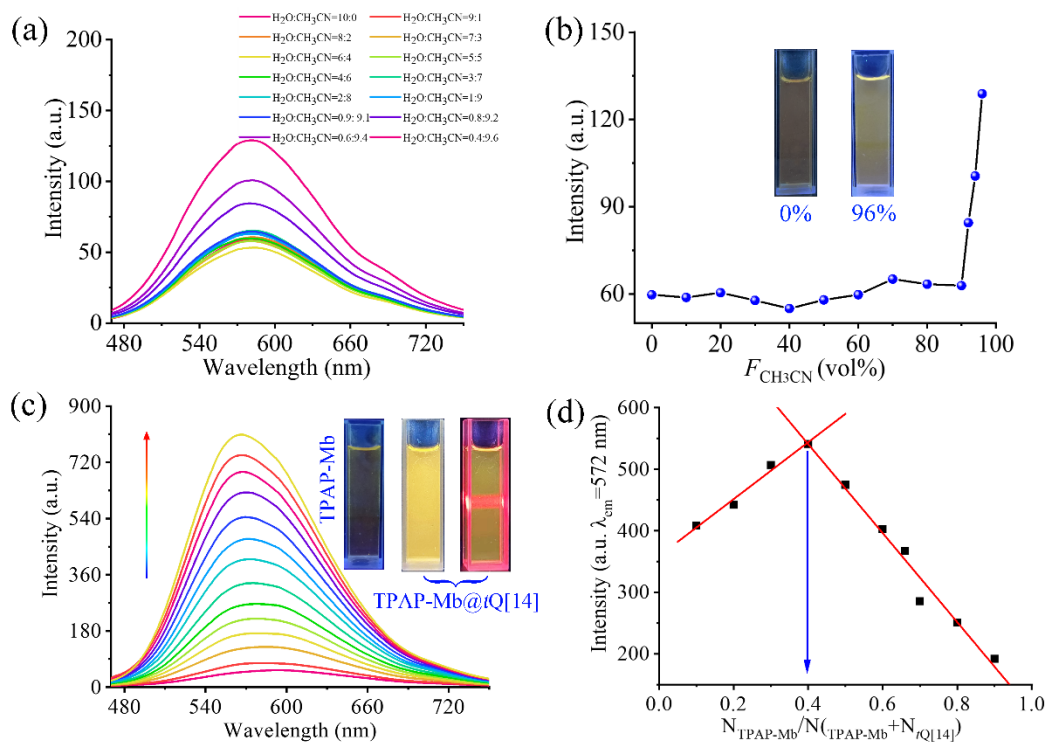


Figure 2. (a, b) The fluorescence spectra of TPAP-Mb in mixed solvents of H₂O/CH₃CN with different ratios, insert: photographs of TPAP-Mb and TPAP-Mb with 96% CH₃CN under UV light irradiation; (c) the fluorescence spectra of TPAP-Mb (20 μM, water) in 0, 0.2, 0.4 ... 3.0 equivalents of tQ[14], insert: photographs of TPAP-Mb, TPAP-Mb@tQ[14] and the Tyndall effect; (d) The Job's plot of TPAP-Mb@tQ[14].

To further accurately express the formation process and structural features of TPAP-Mb@tQ[14], DLS, TEM and SEM were employed. As shown in Figure 3d, dynamic light scattering (DLS) depicts the change in particle size of the polymer during the formation process. The DLS data show that the particle size of TPAP-Mb in the dispersed state in an aqueous solution is 5-8 nm, and the particle size of the aggregates formed after the addition of tQ[14] is 280-410 nm. Furthermore, fluorescent aggregates of TPAP-Mb@tQ[14] were observed by inverted fluorescence microscopy (Figure 3c), while TPAP-Mb at the same concentration showed only a

few faint fluorescent spots (Figure S13). This result further confirms the size change during TPAP-Mb@tQ[14] formation. The morphology of TPAP-Mb@tQ[14] supramolecular polymers was investigated by TEM and SEM experiments. As shown in Figures 3a and 3b, the morphology of TPAP-Mb@tQ[14] is a longitudinal crossed and overlapping meshwork (Figure 3a) with a size of about 174 nm-624 nm. TEM similarly showed TPAP-Mb@tQ[14] as a densely distributed fluffy meshwork (Figure 3b). The reason for the large difference between the DLS and SEM dimensions may be that during the change of environment from the liquid phase to the solid phase in which TPAP-Mb@tQ[14] is located, the complexes may initially form a mesh-like assembly and later fold to form a spherical assembly in order to reduce the surface tension. Based on the above evidence, it is reasonable to speculate that TPAP-Mb@tQ[14] can be assembled to extend into interlaced, crossed and overlapping reticular supramolecular polymers, and a possible assembly mode is proposed in Scheme 1.

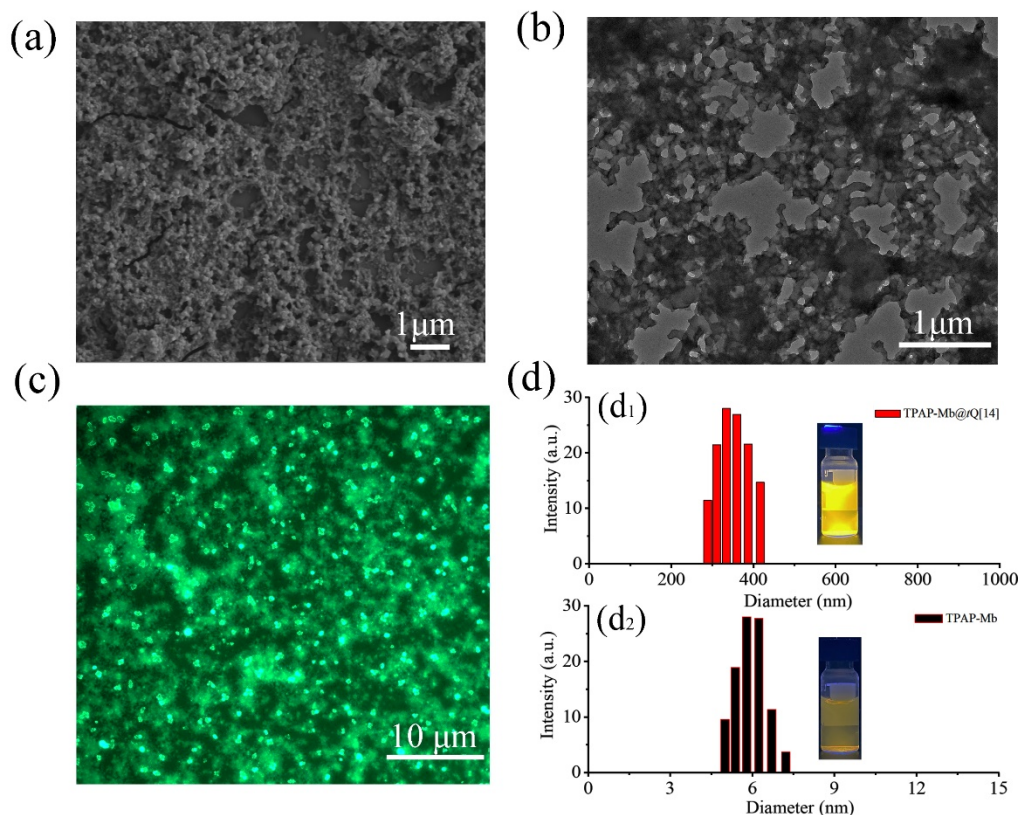


Figure 3 (a, b) The SEM and TEM of TPAP-Mb@tQ[14]; (c) The inverted fluorescent microscope of TPAP-Mb@tQ[14]; (d) The DLS of TPAP-Mb and TPAP-Mb@tQ[14].

Given that TPAP-Mb@tQ[14] possesses good optical properties, the specific recognition performance of TPAP-Mb@tQ[14] for anions in an aqueous solution was investigated by fluorescence experiments. As shown in Figure 4a, different varieties of anions (including F⁻, Cl⁻, Br⁻, I⁻, HIO₃³⁻, SCN⁻, Fe(CN)₆³⁻, SO₄²⁻, H₂PO₄⁻, P₂O₇⁴⁻, S₂O₃²⁻, ClO₄⁻, AC⁻, NO₃⁻, CO₃²⁻, c= 0.1 mM) were added to the aqueous solution of TPAP-Mb@tQ[14] while monitoring changes in the fluorescence spectra. Among the above anions, only Fe(CN)₆³⁻ caused a sharp decrease in the fluorescence of TPAP-Mb@tQ[14] and a change in fluorescence color from bright yellow to dark, while the fluorescence color of the other anions remained essentially unchanged (Figure 4b), indicating that TPAP-Mb@tQ[14] is highly selective for Fe(CN)₆³⁻. Subsequently, fluorescence titration experiments were used to investigate the ability of TPAP-Mb@tQ[14] to detect Fe(CN)₆³⁻. As shown in Figure 4c, the fluorescence intensity of TPAP-Mb@tQ[14] at $\lambda_{em}=572$ nm decreased from 687.54 a.u. to 76.35 a.u. with increasing Fe(CN)₆³⁻ concentration and the detection of limit were calculated based on the $3\sigma/S$ value as 1.64×10^{-7} M ($y=957.7x+38.9$, $R^2>0.99$). This indicates that TPAP-Mb@tQ[14] has potential applications not only for the detection of potential cyanide in water but also shows good anti-interference ability for other anions (Figures S14-S16).

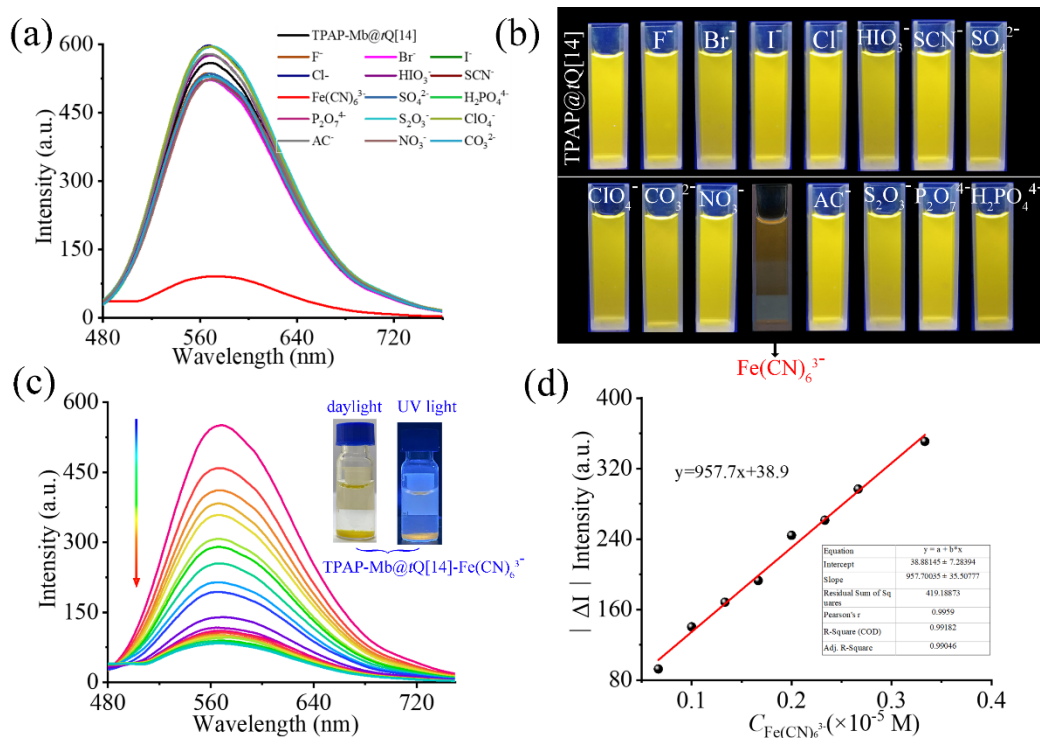


Figure 4 (a) The fluorescence spectra of TPAP-Mb@tQ[14] (20 μM) towards 3 equivalents of different anions at $\lambda_{em}=572$ nm; (b) photographs of the above solutions illuminated by a UV lamp at 365 nm; (c) Fluorescence spectra of TPAP-Mb@tQ[14] (pH=6.75, 20 μM) on increasing the concentration of Fe(CN)₆³⁻ from 0, 6, 12, ... to 80 μM; (d) The LOD plot of TPAP-Mb@tQ[14] in detecting Fe(CN)₆³⁻ in an aqueous solution.

Interestingly, TPAP-Mb@tQ[14] not only specifically recognizes Fe(CN)₆³⁻ but also effectively removes the residual Fe(CN)₆³⁻ from aqueous solutions. Fe(CN)₆³⁻ was gradually added to the TPAP-Mb@tQ[14] solution and left for a time, and a large amount of precipitate appeared at the bottom of the solution. At this time, the color of the solution changed from yellow to clear and transparent, which could be separated by high-speed centrifugation. Subsequently, the liquid phase was subjected to UV-vis and fluorescence spectroscopy, and the results showed that Fe(CN)₆³⁻ was essentially absent in the liquid phase, indicating that TPAP-Mb@tQ[14] could effectively remove Fe(CN)₆³⁻ (Figures S17-S18). To further determine the morphology *etc.* of the precipitate, DLS,

SEM and TEM experiments were employed. As shown in [Figure 5d](#), the DLS shows that after the adsorption of $\text{Fe}(\text{CN})_6^{3-}$, an increasing trend in particle size occurs with a size of 350-510 nm. Meanwhile, SEM and TEM ([Figure 5a, b](#)) together show that the precipitate (TPAP-Mb@tQ[14]- $\text{Fe}(\text{CN})_6^{3-}$) after adsorption of $\text{Fe}(\text{CN})_6^{3-}$ does not change significantly compared to the morphology of TPAP-Mb@tQ[14] and remains as a reticulated porous flocculent structure. It is known that the addition of electrolytes causes colloidal particles to aggregate into larger particles for precipitation.^{43,44} Subsequently, zeta potential experiments were used to investigate the charged nature of individual samples ([Figures S19-S21](#)). In deionized water, the zeta potential of TPAP-Mb@tQ[14] was 24.17 mV, while that of $\text{Fe}(\text{CN})_6^{3-}$ was -30.08 mV, which decreased to -7.7mV as $\text{Fe}(\text{CN})_6^{3-}$ was gradually added to TPAP-Mb@tQ[14].^{44,45} The results indicate that the addition of $\text{Fe}(\text{CN})_6^{3-}$ reduces or neutralizes the charge carried by TPAP-Mb@tQ[14] and the charge in the system is redistributed, leading to the occurrence of coagulation. UV absorption spectroscopy was used to confirm the intrinsic mechanism by which $\text{Fe}(\text{CN})_6^{3-}$ causes the fluorescence quenching of TPAP-Mb@tQ[14].^{46,47} As shown in [Figure 5c](#), the absorption of $\text{Fe}(\text{CN})_6^{3-}$ alone and the emission spectrum of TPAP-Mb@tQ[14] overlapped, while the other anions did not have much overlap ([Figure S22](#)). The effective absorption of $\text{Fe}(\text{CN})_6^{3-}$ hinders the excitation of TPAP-Mb@tQ[14] at 432 nm, so the competitive absorption mechanism between $\text{Fe}(\text{CN})_6^{3-}$ and TPAP-Mb@tQ[14] may be responsible for the quenching effect.

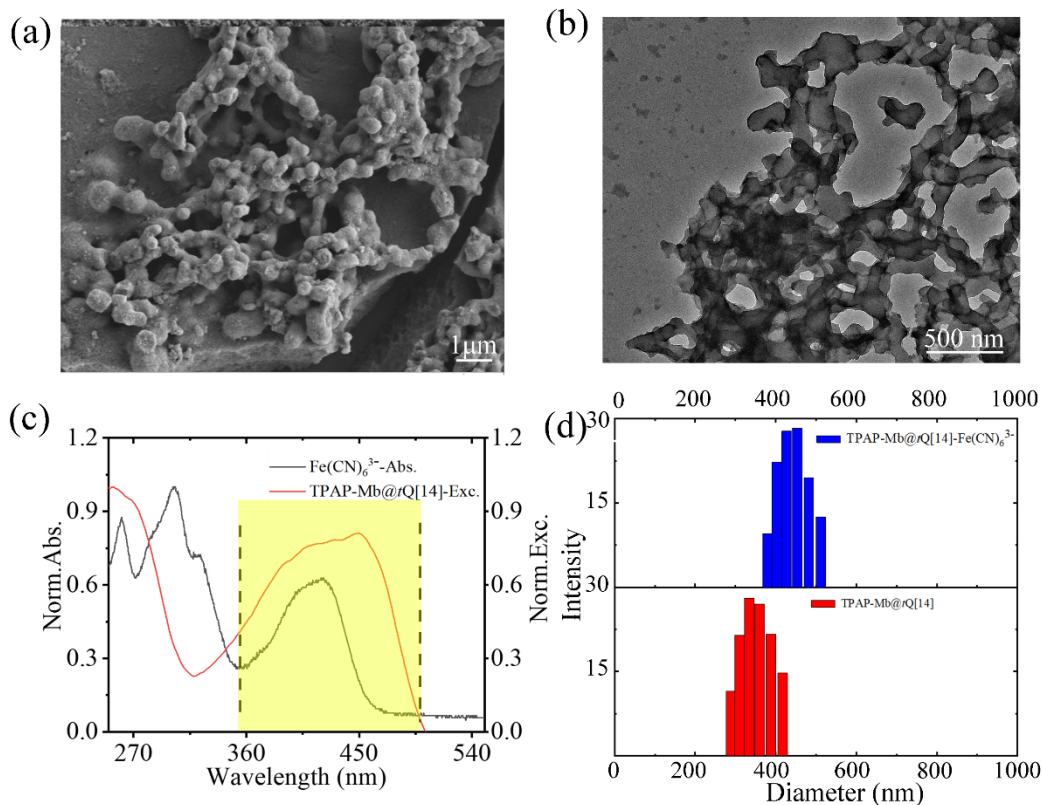


Figure 5. (a, b) The SEM and TEM of TPAP-Mb@*t*Q[14]-Fe(CN)₆³⁻; (c) normalized absorption of Fe(CN)₆³⁻ and excitation spectra of TPAP-Mb@*t*Q[14]; (d) the DLS of TPAP-Mb@*t*Q[14] and TPAP-Mb@*t*Q[14]-Fe(CN)₆³⁻.

To further investigate the ability of TPAP-Mb@*t*Q[14] to remove Fe(CN)₆³⁻ from water, the absorption values of different concentrations of Fe(CN)₆³⁻ were tested and the standard curve was plotted ($y=0.06328x+0.024$, $R^2>0.99$), **Figure 6a**. Subsequently, TPAP-Mb@*t*Q[14] ($c=20 \mu\text{M}$) was added to water containing different concentrations of Fe(CN)₆³⁻. After ultrasonic shaking to make it fully absorbed, the liquid phase was taken to test its absorption value after standing for a few moments. Based on Lambert's law, the residual amount of Fe(CN)₆³⁻ in water was calculated to be $4.78 \mu\text{M}$ (**Figure 6b**) with an average removal rate of 97.38% (**Table S2, Figure S23**), and a decreasing trend in removal rate was observed when the concentration of Fe(CN)₆³⁻ increased to $80 \mu\text{M}$ (**Figure 6c**). In addition, *t*Q[14] as a valuable macrocyclic compound, could be recovered

from acetone/chloroform ($V_{\text{acetone}}: V_{\text{chloroform}}=1:1$) mixture solution by a simple reprocessing experiment with a recovery of 68.3%. (Figure S24, Table S3) The above results have important implications for the detection and removal of potentially highly toxic cyanide in water.

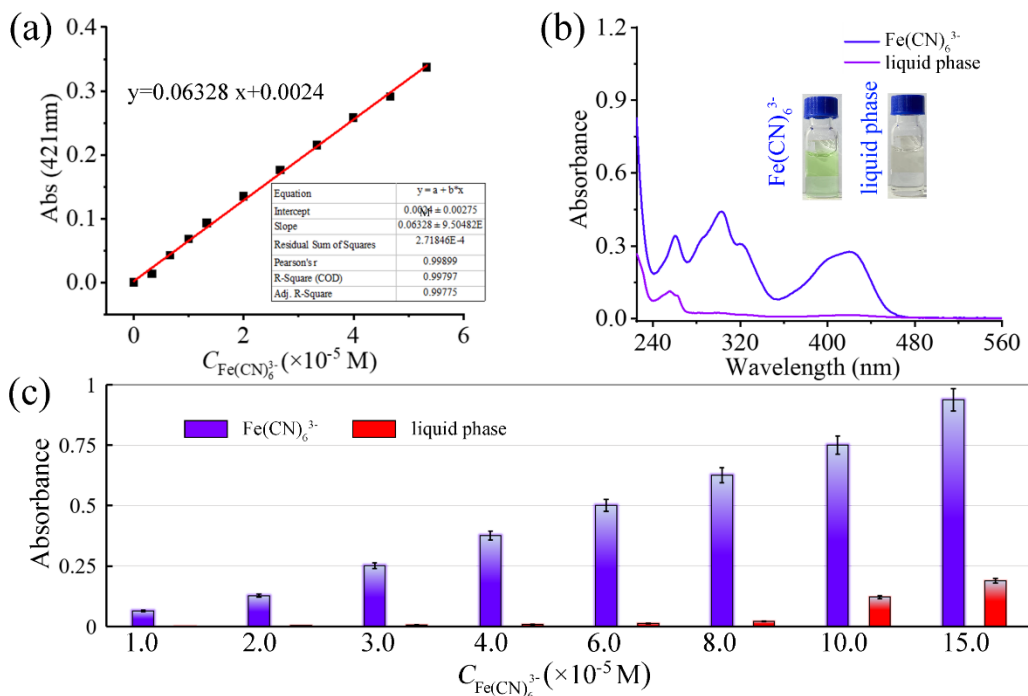


Figure 6 (a) UV absorption standard curve of $\text{Fe}(\text{CN})_6^{3-}$; (b) The UV absorption spectra of liquid phase with $20 \mu\text{M Fe}(\text{CN})_6^{3-}$; (c) Histogram of UV absorption spectra of $\text{Fe}(\text{CN})_6^{3-}$ in the liquid phase before and after the removal.

CONCLUSION

In summary, we have constructed a supramolecular reticulated polymer with an AIE effect based on $t\text{Q}[14]$. The polymer was constructed from the butyl and methylpyridine portions of the three branched arms of TPAP-Mb with $t\text{Q}[14]$ through host-guest interactions and showed bright yellow emission subject to the RiR mechanism. It can detect residual $\text{Fe}(\text{CN})_6^{3-}$ in aqueous solutions with high sensitivity and detection limits up to $1.64 \times 10^{-7} \text{ M}$. More importantly, TPAP-Mb@ $t\text{Q}[14]$ showed the ability to efficient removal of $\text{Fe}(\text{CN})_6^{3-}$ with a removal rate of 97.38%. Meanwhile,

*t*Q[14] can be recycled in acetone/chloroform mixture solution by the use of a high-speed centrifuge. Thus, the present work provides new insights and approaches for *t*Q[14] based AIE supramolecular polymers in solving environmental pollution problems.

AUTHOR INFORMATION

Corresponding Author

* Corresponding author: gyhxxiaoxin@163.com

Author Contributions

The manuscript was written through the contributions of all authors. All authors have approved the final version of the manuscript.

Conflicts of interest

There are no conflicts to declare.

ACKNOWLEDGEMENTS

This work was supported by the National Natural Science Foundation of China (No. 21861011, 21871064), the Innovation Program for High-level Talents of Guizhou Province (No. 2016-5657) the Science and Technology Fund of Guizhou Province (No. 2018-5781). CR thanks the University of Hull for support.

SUPPORTING INFORMATION

Conventional experimental methods, calculation methods, and the characterization of the compounds, *etc.* can be found in the [Supporting Information](#).

REFERENCES

- [1] He, X.; Ewing, A-G. Anionic Species Regulate Chemical Storage in Nanometer Vesicles and Amperometrically Detected Exocytotic Dynamics, *J. Am. Chem. Soc.* 2022, 144, 4310-4314.
- [2] Isom, G-E.; Way, J-L. Effect of Oxygen on Cyanide Intoxication. VI. Reactivation of Cyanide-Inhibited Glucose Metabolism. *J. Pharmacol. Exp. Ther.* 1974, 189, 235.
- [3] Panja, S.; Panjab, A.; Ghosh, K. Supramolecular Gels in Cyanide Sensing: a Review, *Mater. Chem. Front.*, 2021, 5, 584-602.
- [4] Lee, J.; Choudhury, S.; Weingarth, D.; Kim, D.; Presser, V. High-Performance Hybrid Energy Storage with Potassium Ferricyanide Redox Electrolyte, *ACS Appl. Mater. Interfaces*, 2016, 8, 36, 23676-23687.
- [5] Song, W.; Li, J.; Fu, C.; Wang, Z.; Wang, Z.; Wang, Q.; Zhang, X.; Zhou, Y.; Du, X. Low Consumption and Portable Technology for Dithionite Detection Based on Potassium Ferricyanide Differential Spectrophotometry Method in Related Advanced Oxidation Processes, *Environ.*, 2022, 205, 112430.
- [6] Tian, L.; Chen, P.; Jiang, X-H.; Chen, L-S.; Tong, L-L.; Yang, H-Y.; Fan, J-P.; Wu, D-S.; Zou, J-P.; Luo, S-L. Mineralization of Cyanides Via a Novel Electro-Fenton System Generating $\bullet\text{OH}$ and $\bullet\text{O}^{2-}$, *Water Research*, 2022, 209, 117890.
- [7] Kulig, K-W. Department of Health and Human Services. Cyanide Toxicity, U.S., Atlanta, GA, (1991).
- [8] Yang, Y.; Zhao, Q.; Feng, W.; Li, F. Luminescent Chemodosimeters for Bioimaging, *Chem. Rev.* 2013, 113, 192-270.
- [9] Li, S-M.; Zou, J.; Tan, L-F.; Huang, Z-B.; Liang, P.; Meng, X-W. Covalent Organic Frameworks: From Linkages to Biomedical Applications, *Chem. Eng. J.* 2022, 446, 137148.
- [10] Su, X-J.; Li, Z-C.; Feng, J-P.; Hwang, J-Y.; Mo, W.; Ma, S-J.; Lin, H-F. High-Efficiency and Rapid Cyanide Removal in SPL Derived from Aluminum Electrolysis Production Under Microwave and Sensitizer Synergistic Action, *J. Clean. Prod.*, 2022, 365, 132691.

- [11] Long, L-L.; Huang, M.; Wang, N.; Wu, Y.; Wang, K.; Gong, A.; Zhang, Z.; Sessler, J-L. A Mitochondria-Specific Fluorescent Probe for Visualizing Endogenous Hydrogen Cyanide Fluctuations in Neurons, *J. Am. Chem. Soc.* 2018, 140, 1870-1875.
- [12] Xu, J.; Qu, K.; Zhao, J.; Jian, X.; Gao, Z.; Xu, J.; Song, Y-Y. In Situ Monitoring of the “Point Discharge” Induced Antibacterial Process by the Onsite Formation of a Raman Probe, *Anal. Chem.*, 2020, 92, 2323-2330.
- [13] Magotra, V-K.; Lee, S-J.; Kang, T-W.; Inamdar, A-I.; Kim, D-Y.; Im, H.; Jeon, H-C. High Power Generation with Reducing Agents Using Compost Soil as a Novel Electrocatalyst for Ammonium Fuel Cells, *Nanomaterials*, 2022, 12, 1281.
- [14] Prasser, Q.; Steinbach, D.; Münch, A-S.; Neubert, R.; Weber, C.; Uhlmann, P.; Mertens, F.; Plampe, F-A. Interfacial Rearrangements of Block Copolymer Micelles Toward Gelled Liquid-Liquid Interfaces with Adjustable Viscoelasticity, *Small*, 2022, 2106956.
- [15] Guidelines for Drinking-Water Quality, World Health Organization: Geneva, 1996.
- [16] Na, M.; Chen, Y.; Han, Y.; Ma, S.; Liu, J.; Chen, X. Determination of Potassium Ferrocyanide in Table Salt and Salted Food Using a Water-Soluble Fluorescent Silicon Quantum Dots, *Food Chem.* 2019, 288, 248-255.
- [17] Walker, M. K.; Rinko, F.; Lee, J.; Wilson, E.; Ito, K.; Asano, R.; Ikebukuro, K.; LaBelle, J.; Sode, K. Development of a POCT Type Insulin Sensor Employing Anti-insulin Single Chain Variable Fragment Based on Faradaic Electrochemical Impedance Spectroscopy Under Single Frequency Measurement, *Biosens Bioelectron*, 2022, 200, 113901.
- [18] Xue, X.; Gao, M.; Rao, H.; Luo, M.; Wang, H.; An, P.; Feng, T.; Lu, X.; Xue, Z.; Liu, X. Photothermal and Colorimetric Dual Mode Detection of Nanomolar Ferric Ions in Environmental Sample Based on in Situ Generation of Prussian Blue Nanoparticles, *Anal. Chim. Acta* 2020, 1105, 197-207.
- [19] Lin, Q.; Guan, X-W.; Zhang, Y-M.; Wang, J.; Fan, Y-Q.; Yao, H.; Wei, T-B. Spongy Materials Based on Supramolecular Polymer Networks for Detection and Separation of Broad-Spectrum Pollutants, *ACS Sustainable Chem. Eng.* 2019, 7, 14775.

- [20] Yao, H.; Zhou, Q.; Zhang, Y.; Hu, Y.; Kan, X.; Chen, Y.; Gong, G.; Zhang, Q.; Wei, T.; Lin, Q. Supramolecular Polymer Materials, Based on Pillar[5]arene: Ultrasensitive Detection and Efficient Removal of Cyanide, *Chin. Chem. Lett.*, 2020, 31, 1231.
- [21] Shen, H-Q.; Liu, C.; Zheng, J.; Tao, Z.; Nie, H-G.; Ni, X-L. Cucurbit[8]uril-Assisted Nucleophilic Reaction: A Unique: Supramolecular Approach for Cyanide Detection and Removal from Aqueous Solution, *ACS Appl. Mater. Interfaces* 2021, 13, 55463-55469.
- [22] Xu, C-G.; Wu, T.; Duana, L-Z.; Zhou, Y-M. A Naphthalimide-Derived Hypochlorite Fluorescent Probe from ACQ to AIE Effect Transformation, *Chem. Commun.*, 2021, 57, 11366-11369.
- [23] Xu, L-J.; Jiang, X-P.; Liang, K. Gao, M.; Kong, B. Frontier Luminous Strategy of Functional Silica Nanohybrids in Sensing and Bioimaging: From ACQ to AIE, *Aggregate*, 2022, 3, 121
- [24] Feng, E.; Jiao, L.; Tang, S.L.; Chen, M-M.; Lv, S-B.; Liu, D-P.; Song, J-T. Zheng, D-Y.; Peng, X-J. Song, F-L. Anti-Photobleaching Cyanine-Based Nanoparticles with Simultaneous PET and ACQ Effects for Improved Tumor Photothermal Therapy, *Chem. Eng. J.*, 2022, 432, 134355.
- [25] Hong, Y-Y.; Lam, Jacky, W-Y.; Tang, B-Z. Aggregation-Induced Emission, *Chem. Soc. Rev.*, 2011, 40, 5361-5388.
- [26] Rizzo, C.; Marullo, S.; Feroci, M.; Accurso, V.; D'Anna, F. Insights into The Effect of The Spacer on The Properties of Imidazolium Based AIE Luminogens, *Dyes and Pigments* 2021, 186, 109035.
- [27] D'Anna, F.; Rizzo, C.; Vitale, P.; Marullo, S.; Ferrante, F. Supramolecular Complexes Formed by Dimethoxypillar[5]arenes and Imidazolium Salts: a Joint Experimental and Computational Investigation, *New J. Chem.* 2017, 41, 12490.
- [28] Dai, D-H.; Li, Z.; Yang, J.; Wang, C-Y.; Wu, J-R.; Wang, Y.; Zhang, D-M.; Yang, Y-W. Supramolecular Assembly-Induced Emission Enhancement for Efficient Mercury(II) Detection and Removal, *J. Am. Chem. Soc.*, 2019, 141, 11, 4756-4763.

- [29] Wang, P.; Liang, B.; Xia, D. A Linear AIE Supramolecular Polymer Based on a Salicylaldehyde Azine-Containing Pillararene and Its Reversible Cross-Linking by CuII and Cyanide, *Inorg. Chem.*, 2019, 58, 2252-2256.
- [30] Yao, H.; Zhou, Q.; Zhang, Y-M.; Hu, Y-P.; Kan, X-T.; Chen, Y-Y.; Gong, G-F.; Zhang, Q-P.; Wei, T-B.; Lin, Q. Supramolecular Polymer Materials Based on Pillar[5]arene: Ultrasensitive Detection and Efficient Removal of Cyanide, *Chin. Chem. Lett.*, 2020, 31, 1231-1234.
- [31] Wang, P.; Cao, S-X.; Yin, T.; Ni, X-l. Unprecedented Tunable Hydrophobic Effect and Anion Recognition Triggered by AIE with Hofmeister Series in Water, *Chin. Chem. Lett.*, 2021, 32, 1679-1682.
- [32] Zhang, W.; Luo, Y.; Ni, X-L.; Tao, Z.; Xiao, X. Two-Step, Sequential, Efficient, Artificial Light-Harvesting Systems Based on Twisted Cucurbit[14]uril for Manufacturing White Light Emission Materials, *Chem. Eng. J.*, 2022, 446, 136954.
- [33] Zhang, W.; Luo, Y.; Zhao, J.; Lin, W-H.; Ni, X-L.; Tao, Z.; Xiao, X. TQ[14]-Based AIE Supramolecular Network Polymers as Potential Bioimaging Agents for the Detection of Fe³⁺ in Live HeLa Cells, *Sens Actuators: B. Chem.*, 2022, 354, 131189.
- [34] Zhang, W.; Luo, Y.; Yang, M-X.; Li, W-H.; Redshaw, C.; Ni, X-L.; Huang, Y.; Tao, Z.; Xiao, X. Twisted cucurbit[14]uril: A New Type of CTE Macrocyclic for Fe³⁺ Sensing, *Microchem. J.*, 2022, 178, 107364.
- [35] Luo, Y.; Zhang, W.; M. Yang, X.; Feng, X-H.; Redshaw, C.; Li, Q.; Tao, Z.; Tao, X. A Twisted Cucurbit[14]Urill-Based Fluorescent Supramolecular Polymer Mediated by Metal Ion, *Macromolecules*, 2022, 55, 1642-1646.
- [36] Kim, J.; Jung, I-S.; Kim, S-Y.; Lee, E.; Kang, J- K.; Sakamoto, S.; Yamaguchi, K.; Kim, K. New Cucurbituril Homologues: Syntheses, Isolation, Characterization, and X-ray Crystal Structures of Cucurbit[n]uril (n = 5, 7, and 8), *J. Am. Chem. Soc.*, 2000, 122, 540-541.

- [37] Nie, H-G. Zhan, W.; Ni, X-L.; Liu, Y. Assembly and Applications of Macrocyclic-Confinement-Derived Supramolecular Organic Luminescent Emissions from Cucurbiturils, *Chem. Rev.* 2022, 122, 9, 9032-9077.
- [38] Ni, X-L.; Xiao, X.; Cong, H.; Zhu, Q-J.; Xue, S-F.; Tao, Z. Self-Assemblies Based on the “Outer-Surface Interactions” of Cucurbit[n]urils: New Opportunities for Supramolecular Architectures and Materials, *Acc Chem Res*, 2014, 47: 1386-1395.
- [39] Liu, M.; Chen, L-X.; Shan, P-H.; Lian, C-J.; Zhang, Z-H.; Zhang, Y-Q.; Tao, Z.; Xiao, X. Pyridine Detection Using Supramolecular Organic Frameworks Incorporating Cucurbit[10]uril, *ACS Appl. Mater. Inter*, 2021, 13, 7434-7442.
- [40] Luo, Y.; Zhang, W.; Liu, M.; Zhao, J.; Fan, Y.; Bian, B.; Tao, Z.; Xiao, X. A Supramolecular Fluorescent Probe Based on Cucurbit[10]uril for Sensing the Pesticide Dodine, *Chin. Chem. Lett*, 2021, 32, 367-370.
- [41] Yang, D.; Liu, M.; Xiao, X.; Tao, Z.; Redshaw, C. Polymeric Self-assembled Cucurbit[n]urils: Synthesis, Structures and Applications, *Coord. Chem. Rev*, 2021, 434, 213733.
- [42] Gao, R-H.; Huang, Y.; Chen, K.; Tao, Z. Cucurbit[n]uril/Metal Ion Complex-based Frameworks and Their Potential Applications. *Coord. Chem. Rev*, 2021, 437, 213741.
- [43] Luo, Y.; Gan, S-Q.; Zhang, W.; Jia, M-H.; Chen, L-X.; Redshaw, C.; Tao, Z.; Xiao, X. A New Cucurbit[10]uril-based AIE Fluorescent Supramolecular Polymer for Cellular Imaging, *Mater. Chem. Front.*, 2022, 6, 1021-1025.
- [44] Li, H- L. Chen, J.; Peng, C-L.; Min, F-F.; Song, S-X. Salt Coagulation or Flocculation? In Situ Zeta Potential Study on Ion Correlation and Slime Coating with the Presence of Clay: A case of Coal Slurry Aggregation, *Environ.*, 2020, 189, 109875.
- [45] Dorothy, W.; Skaf, Vito L.; Punzi, Javaz T. Rolle, Elizabeth Cullen, Impact of Moringa Oleifera Extraction Conditions on ZetaPotential and Coagulation Effectiveness, *J. Environ. Chem. Eng.*, 2021, 9, 104687.

- [46] Liu, W. Diao, H-P.; Chang, H-H.; Wang, H-J.; Li, T-T.; Wei, W-L. Green Synthesis of Carbon Dots from Rose-heart Radish and Application for Fe³⁺Detection and Cell Imaging, *Sens Actuators B Chem*, 2017, 241, 190-198.
- [47] Yao, Q.F.; Lü, B-Z.; Ji, C-D.; Cai, Y.; and Yin, M-Z.; Supramolecular Host-Guest System as Ratiometric Fe³⁺ Ion Sensor Based on Water-Soluble Pillar[5]arene, *ACS Appl. Mater. Interfaces* 2017, 9, 36320-36326.